



# Green Synthesis, Characterization, and Application of *Ascophyllum Nodosum* Silver Nanoparticles

Sunil Kumar Mishra<sup>1</sup> · Saket Sinha<sup>1</sup> · Amit Kumar Singh<sup>1</sup> · Prabhat Upadhyay<sup>2</sup> · Diya Kalra<sup>3</sup> · Pradeep Kumar<sup>4</sup> · Kavindra Nath Tiwari<sup>4</sup> · Rajan Singh<sup>5</sup> · Rakesh Kumar Singh<sup>5</sup> · Arvind Kumar<sup>6</sup> · Alok Tripathi<sup>6</sup> · Brijesh Singh Chauhan<sup>7</sup> · S. Srikrishna<sup>7</sup>

Received: 16 June 2022 / Revised: 23 December 2022 / Accepted: 22 February 2023 / Published online: 7 March 2023  
© The Author(s), under exclusive licence to The Regenerative Engineering Society 2023

## Abstract

**Purpose** Green nanotechnology as a field has emerged and gained popularity amongst biologists due to its cost-effective and environment-friendly advancements. The most preferred is the biological method which involves plants and their extracts.

**Methods** The silver nanoparticles were synthesized by a sunlight-driven aqueous extract (AE) of whole plant powder of *Ascophyllum nodosum*. Advanced techniques like high-resolution scanning electron microscopy (HRSEM), energy dispersive X-ray (EDX), high-resolution transmission electron microscopy (HRTEM), and particle size analysis were used to determine the nature of nanoparticles. Antioxidant, anti-fungal, and anti-leishmanial activities were evaluated.

**Result** The techniques confirmed the formation of spherical particles of the desired range of size. Silver nanoparticles exhibited a much greater DPPH (2,2-diphenyl-1-picryl-hydrazine-hydrate) radical scavenging activity which was almost six to seven folds more than that exhibited by the AE alone. The anti-leishmanial and cytotoxic activities were evaluated on *Leishmania donovani* promastigote and amastigote.

**Conclusion** The synthesized AgNPs showed remarkable DPPH radical scavenging ability owing to their antioxidant properties. The anti-leishmanial activity was exceptionally viable in both AE and AgNPs. The findings all together support the tendency of *Ascophyllum nodosum* to efficiently synthesized AgNPs which could be utilized for its anti-leishmanial properties.

**Keywords** Antioxidant · Silver nanoparticle · Anti-leishmanial activity · Cytotoxicity · *Ascophyllum nodosum*

## Key Points

1. Aqueous extract of *A. nodosumas* served as a capping and stabilizing agent for photo-induced synthesis of AgNPs of 30–60 nm in size.
2. The tendency of *Ascophyllum nodosum* to efficiently synthesize AgNPs which could be utilized for its anti-leishmanial properties.

✉ Sunil Kumar Mishra  
skmishra.phe@itbhu.ac.in

<sup>1</sup> Department of Pharmaceutical Engineering & Technology, Indian Institute of Technology, Banaras Hindu University, Varanasi, India

<sup>2</sup> Molecular Science Lab, National Institute of Immunology, New Delhi, India

<sup>3</sup> Department of Biotechnology, Jamia Hamdard University, New Delhi, India

## Introduction

Nanotechnology deals with atoms, molecules, and macromolecules with a size range of 1 to 100 nm and involves developing materials or devices within that size. Research on nanoparticles has gained huge attention in recent years due to its widespread utility in fields ranging from electronics to agriculture. The main characteristics of NPs are responsible for increasing surface area, volume, and absorption due to

<sup>4</sup> Department of Botany, MMV, Banaras Hindu University, Varanasi, India

<sup>5</sup> Department of Biochemistry, Institute of Science, Banaras Hindu University, Varanasi, India

<sup>6</sup> School of Biotechnology, Institute of Science, Banaras Hindu University, Varanasi, India

<sup>7</sup> Cell and Neurobiology lab Department of Biochemistry, Institute of Science, Banaras Hindu University, Varanasi, India

the reduction of size and optical, chemical, physical, and magnetic properties [1]. AgNPs have proven to be the most efficient of all nano-sized metallic particles and are now considered to be a vital anti-bacterial agent. A pool of applications makes AgNPs the widely accepted nanomaterial in the pharmaceutical industry, optical sensors, domestic and healthcare-related products, consumer products, diagnostics, medical device coatings, the food industry, and cosmetics. Commercially, they are also used nowadays in sporting equipment, where silver-embedded fabrics are used [2].

Various methods for the production of nanoparticles are reported in the literature. Although the chemical method is till-date the most popular approach for producing nanoparticles, it involves the use of toxic chemicals, making the entire process hazardous and expensive. For the production of AgNPs, a more cost-effective, commercially viable as well as environmentally, the clean route is yet to be discovered [3]. For their high utility in the field of medicine, environmentally and biologically safe protocols need to be followed. These concerns led to the development of procedures that today we call non-toxic “green syntheses” [4]. Green here refers to the usage of plants or their extracts as reducing and stabilizing agents in place of poisonous toxic chemicals for the biosynthesis of nano-sized particles [5].

The brown seaweed *Ascophyllum nodosum* (rockweed) is predominantly found on the rocky intertidal shores of the Atlantic region of Nova Scotia and New Brunswick, Canada. The species is confined to the North Atlantic region, which extends from the Arctic Circle to New Jersey in North America [6]. *A. nodosum* is considered an economically important seaweed, as it is harvested every year for its use in alginates (wound dressings), as a fertilizer, and as an animal meal. Furthermore, evaluation of antioxidant properties [7], antimicrobial properties [8], and neuroprotective [9] have been performed on the rockweed, and significant results were reported [10]. Thus, we selected the seaweed *A. nodosum* for the first time to synthesize the AgNPs in a green, eco-friendly way through a photo-induced method. The synthesized AgNPs were screened for their DPPH radical scavenging ability, parallel with the AE of *A. nodosum*. The anti-leishmanial activity was investigated on amastigote and promastigote cells for both AgNPs and AE.

## Material and Methods

The whole plant powder of the seaweed *A. nodosum* was obtained from Canada and is identified in the Department of Botany, Banaras Hindu University, and authenticated for further study. Analytical grade silver nitrate ( $\text{AgNO}_3$ ), DPPH [1, 1-diphenyl-2-picryl hydrazyl], and DMSO (dimethyl sulfoxide) were obtained from Merck chemicals. The authentication of anti-leishmanial activity of AgNPs and AE

was evaluated on the cloned line of *L. donovani* (MHOM/IN/1983/AG83) promastigotes. Mueller Hinton agar and broth media (Himedia Lab Ltd., Mumbai) were used to study culture growth activity. All the glassware was washed with distilled water and dried properly.

## Preparation of Plant Extract

A total of 30 g of the whole plant powder of *Ascophyllum nodosum* was weighed and boiled in 100 ml of double-distilled deionized water. The boiling was continued for around 30–35 min. Then the excess water was decanted and filtered through Whatman Filter Paper No. 1. The filtrate was then evaporated, to remove the solvent and obtain the crude extract. The collected crude extracted was dried well and stored at 4 °C.

## Photo-Induced Synthesis of Silver Nanoparticles (AgNPs)

A reaction mixture was prepared by taking 0.1 ml AE with 10 ml of 1 mM  $\text{AgNO}_3$  solution. The concentration of the AE was maintained at 1 mg/ml. The biosynthesis of nanoparticles was done by exposing the reaction mixture to the sunlight for a duration of 5–60 min at 5 min intervals. The intensity of the incident solar light was found as 63000lx. Meanwhile, the UV-absorbance was also measured with respect to time at 200 to 800 nm using the Shimadzu UV-1800 instrument.

## Effect of Varying Concentrations of $\text{AgNO}_3$

The effect of different concentrations of  $\text{AgNO}_3$  on the formation of nanoparticles was also studied. The concentration of  $\text{AgNO}_3$  was made to vary from 0.5 to 3.0 mM with an increasing difference of 0.5 mM. In contrast, each reaction mixture kept the AE concentration constant (1 mg/ml). Various reaction mixtures of multiple  $\text{AgNO}_3$  concentrations with AE were exposed to sunlight for about 5 min. In this way, the effect of altered concentrations of  $\text{AgNO}_3$  for the AgNP synthesis is studied by UV-visible absorption spectroscopy.

## Effect of the Aqueous Extract (AE) Inoculum Dose

Similarly, the effect of different quantities of AE on the synthesis of nanoparticles was studied by keeping the concentration of  $\text{AgNO}_3$  constant (1 mM). The initial amount of AE was standardized by altering its volume from 200 to 2000  $\mu\text{l}$ , for a common exposure of 5 min in the sunlight. The optimum dose of the AE was confirmed by following the same procedure of nano synthesis.

## Characterization of the Green Synthesized AgNPs

The Fourier-transform infrared spectroscopy (FTIR) spectra were attained from Perkin Elmer Spectrophotometer-2, Germany, by employing the KBr pellet technique, in the wave number range of 450 to 4000  $\text{cm}^{-1}$ . The optical properties of the biocompatible nanotized silver particles were evaluated using UV-visible spectroscopy (Shimadzu UV-1800). High-resolution scanning electron microscopy (HRSEM) (Nova Nano SEM450) was performed to analyze the morphology of the nanoparticles at an accelerating voltage of 10 kV. The beam current was kept at 1 nA, with an average measuring time of 7 s. The elemental composition was confirmed with the energy-dispersive X-ray (EDX) detector, which was equipped with the HRSEM. High-resolution transmission electron microscopy (HRTEM; TECHNI G2 20 TWIN; FEI), at an accelerating voltage of 200 kV, was used in studying the size and morphology of AgNPs. “Image J” software was used to calculate the average particle size. Particle size analysis of biosynthesized AgNPs was obtained using dynamic light scattering Malvern-Zeta sizer (Particle Systems, Nanoplus, Shimadzu). The XRD pattern was checked by an X-ray diffractometer (Rigaku Miniflex 600) installed with a Cu  $K\alpha$  radiation source and a Ni filter. Spectra were performed in the  $2\theta$  region in the range of 20–80° at the scanning rate of 2°  $\text{min}^{-1}$ . The crystalline nature of the particles was authenticated using the selected area electron diffraction (SAED) pattern. Spectroscopy was done after the photo-synthesis mentioned above at 200–700 nm. The surface texture of AgNPs was analyzed using atomic force microscopy (NT-MDT, Russia). The images were processed using NOVA software. AgNPs obtained from AE were analyzed for their chemical state and near-surface composition using X-ray photoelectron spectroscopy (XPS). Specific groups of macromolecules such as P=S, aromatic rings, C–O, and C=O were recognized and characterized by XPS.

## DPPH Radical Scavenging Assay

This study was performed to find out the antioxidant potential of the synthesized AgNPs, with respect to the original AE. Hence, the DPPH radical scavenging activity of both AE of the *A. nodosum* and the green synthesized AgNPs was studied, and the results were compared. DPPH solution of 0.004% was prepared in distilled water. A total of 2.96 ml of DPPH solution was mixed with various concentrations of samples (50–700  $\mu\text{g/ml}$ ). The solution was then kept at room temperature in dark conditions for 20 min [11]. The absorbance of the reaction mixture was checked after 20 min with a UV-Vis spectrophotometer at a wavelength of 517 nm, where DPPH was used as a control. The following equation was used for the calculation of percentage inhibition:

$$\left[ \frac{(\text{Absorbance}_{\text{control}} - \text{Absorbance}_{\text{sample}})}{(\text{Absorbance}_{\text{control}})} \right] \times 100$$

The mean and standard deviation (SD) were calculated by repeating all the experiments thrice. *P* values of  $\leq 0.001$  were considered significant. The half maximal inhibitory concentration ( $\text{IC}_{50}$ ) was calculated by comparing it with that of the standard (ascorbic acid is taken as standard), by linear regression analysis.

## In-Vitro Antifungal Activity

The main aim of this study is to compare the antifungal potential of both the AgNPs as well as AE with that of the standard anti-fungal drug (Fluconazole). Week-old cultured strains of *Candida albicans* (ATCC 90028) and *Candida tropicalis* (ATCC 750) were selected for this study. The study was conducted by following the CLSI guidelines M44-A2. The standard inoculum is prepared by treating the stains with 5 ml of sterile saline, and the turbidity is maintained to be at Mac Farland’s scale of 0.5 ( $10^6$  C.F.U/ml) [12].

## Disc Diffusion Method

In vitro antifungal activity was assessed by performing an agar disc diffusion assay [13]. About 0.2 ml suspension of the prepared standard inoculum was spread on the surface of Mueller Hinton Agar media (MHA media), with a sterile cotton swab. Stock solutions of 100  $\mu\text{g/ml}$  of the test samples were prepared in DMSO. A total of 5  $\mu\text{l}$  of the stock solution was impregnated into the well-sterilized Whatman No. 1 Paper disc of 6 mm diameter. These paper discs containing the samples (AE and AgNPs) were placed on the inoculated MHA media. A standard anti-fungal disc (Fluconazole 10 mg/disc, HiMedia) was also placed. The experiment was performed in triplicates aseptically, and all the plates were incubated at 25 °C for 48 h. The diameter of the zone of inhibition was measured to assess the susceptibility.

## Determination of MFC and MIC

The minimum inhibitory concentration (MIC) and minimum fungicidal concentration (MFC) were measured using the broth microdilution method [14, 15]. An initial stock of 4 mg/ml of the samples was made in DMSO. A total of 1 ml of Mueller Hinton Broth solution was added to 10 sterile clean tubes. Two-fold serial dilutions (2000  $\mu\text{g/ml}$ , 1000  $\mu\text{g/ml}$ , 500  $\mu\text{g/ml}$ , 250  $\mu\text{g/ml}$ , 125  $\mu\text{g/ml}$ , 62.5  $\mu\text{g/ml}$ , 31.2  $\mu\text{g/ml}$ , 15.6  $\mu\text{g/ml}$ ) of the test samples were added to the tubes. Now, 1 ml of the filtrate suspension of the standard inoculum, containing the fungal strains was added to all the tubes. One tube was labeled as antifungal control (AC) which received the stock concentration of the test antifungal sample, but inoculum was not added. Another tube was

labeled as growth control (GC) in which no test sample was added. All the tubes were incubated at 37 °C for 24 h, and the growth of the organisms was examined. The MIC was verified by observing the minimum concentration that inhibits the visible growth (cloudiness) in the tubes.

For the checking, the minimum fungicidal concentration (MFC), the contents of the selective tubes (2nd last non-visible tube to 2nd visible tube) are sub-cultured into the Mueller Hinton Broth, which do not contain any anti-fungal test samples. Then they are inoculated into the MHA media for plate culturing, by drop method using sterile micropipettes. Culture plates were kept at 37 °C for 24 h.

### Cytotoxicity Activity

Cervical dislocation of Balb/c mice was carried out, and the spleen was dissected from sacrificed mice. Spleen was washed with cold phosphate-buffered saline (PBS), and the cell suspension was made by chopping the tissues in incomplete Dulbecco's modified eagles' medium (DMEM). RBCs' lysis was carried out in the presence of RBCs lysis buffer (1 mM NaHCO<sub>3</sub>, 0.15 M NH<sub>4</sub>Cl, 0.1 mM EDTA at pH 7.4). An incomplete DMEM medium was washed twice to wash the isolated splenocytes and centrifuged at a speed of 2000 rpm for 10 min at 4 °C. The obtained pellet was re-suspended in an incomplete DMEM medium. The viability of cells was checked by trypan blue exclusion assay using a hemocytometer. Viable cells of concentration  $2 \times 10^6$  cells/ml were seeded in a 6-well culture plate and kept in a CO<sub>2</sub> incubator for cells to grow properly up to 2 h at 37 °C and 5% CO<sub>2</sub>. All the animal ethical rules were followed as per the guidelines of the animal ethical committee of Banaras Hindu University, Varanasi, UP, India.

### Cytotoxicity Assay with Plants Extract

Splenocyte cells were treated with various concentrations of prepared plant extract (0, 20, 80, 100, 200, and 400 µg/ml). Cells were incubated for 1 h in a CO<sub>2</sub> incubator at 37 °C and 5% CO<sub>2</sub> after the treatment. Cells were collected by trypsinization from the culture plate and subjected to centrifugation at 2000 rpm at 4 °C for 10 min for pellet formation. The pellet was re-suspended in the incomplete DMEM medium, and the percent cell viability was calculated using a trypan blue exclusion assay using hemocytometer.

### Cytotoxicity Assay with Synthesized Nanoparticles

Splenocyte cells were treated with different concentrations of synthesized nanoparticles (0, 20, 40, 80, 100, and 200 µg/ml). Cells were incubated for 1 h in a CO<sub>2</sub> incubator at 37 °C and 5% CO<sub>2</sub> after the treatment. Cells were collected by trypsinization from the culture

plate and subjected to centrifugation (2000 rpm/4 °C/10 min) for pellet formation. Pellet was re-suspended in the incomplete DMEM medium and percent cell viability was totally led by trypan blue exclusion assay using hemocytometer.

## Anti-Leishmanial Activity

### Culture Conditions

*L. donovani* promastigote parasites were grown in vitro in Dulbecco's Modified Eagle's Medium (DMEM; Invitrogen, USA) modified to contain 4 mM L-glutamine, 4500 mg/L glucose, 1 mM sodium pyruvate, and 1500 mg/L sodium bicarbonate supplemented with 10% fetal bovine serum (FBS) and antibiotics (Streptomycin 100 µg/mL, penicillin 100 U/ml, gentamycin 20 µg/ml, Sigma, USA) at pH 7.2 and finally incubated in bio-oxygen demand (BOD) incubator at 26 °C. Mouse macrophages, RAW 264.7, were cultured and allowed to adhere in the 24 well plates at a concentration of  $5 \times 10^5$  cells/100 µL/well in DMEM medium having 10% FBS, 1% streptomycin, penicillin, and incubated at 37 °C in 5% CO<sub>2</sub> incubator. Phosphate buffered saline—pH 7.2 (25 °C)—was used to wash the plates.

### Cytotoxicity Assay (Anti-Leishmanial)

For evaluation of cytotoxicity of test compounds against mice macrophages cell line, RAW 264.7 were cultured in DMEM containing 10% FBS at 37 °C in a 5% CO<sub>2</sub> atmosphere. After that, the macrophages were seeded in a 96-well microtiter plate at a concentration of  $1 \times 10^6$  cells/ml in the presence of compounds which were two-fold serially diluted over 8 concentration points ranging from 100 µg so that the final concentration of compounds became range from 50 to 0.39 µg/ml and incubated at 37 °C in 5% CO<sub>2</sub> atmosphere. Miltefosine, a commercially available anti-leishmanial drug, was used for standard control. Cells that were not treated with any drug were taken as control. Furthermore, the S.I. was calculated by the ratio between CC<sub>50</sub> and IC<sub>50</sub> of macrophage amastigote.

## Determination of Effects of AgNPs on Proliferation, Infectivity, and Cell Viability of *L. Donovani*

### Antiamastigote Activity Assay

Macrophages (RAW 264.7) were infected by flagellated promastigote form of *L. donovani*. Post-infection, promastigotes were phagocytosed and transformed into the non-motile amastigotes form of *L. donovani*. The culture plate was incubated for 4–6 h; after completion of incubation, the culture plate was given a one-time wash. Furthermore,

the test compounds (200  $\mu\text{L}$ ) were added two-fold serially diluted over 8 concentrations ranging from 100 to 0.78  $\mu\text{g}/\text{mL}$  and then incubated for 48 h. After 48 h, bio-evaluation of anti-leishmanial activity towards intracellular amastigotes was measured by using direct counting assays following fixation and Giemsa staining. All assays were performed in triplicates, and drug activity was analyzed under phase contrast microscopy.

### In Vitro Promastigote Assay

Promastigotes in their logarithmic phase were seeded in a 96-well culture plate ( $1 \times 10^6$  cells 100  $\mu\text{L}/\text{well}$ ) for identifying  $\text{IC}_{50}$  of synthesized particles. The plate was seeded without (control wells) or with 100  $\mu\text{L}$  of reaction mixture per well such that the final concentration of samples in the well varied from 100 to 0.78  $\mu\text{g}/\text{mL}$  (serial dilution) and incubated for 48 h. Furthermore, to determine the inhibition percentage of the respective test compound, MTT (3-(4, 5-dimethylthiazolyl-2)-2, 5-diphenyltetrazolium bromide) assay was done. This, MTT assay was used to check the presence of viable cells, after the treatment of the test compound. The mechanism behind this assay is the conversion of MTT to formazan by mitochondrial enzymes served as an indicator of cell viability. The amount of formazan produced indicates the viable cells with an active metabolism. Briefly, MTT (5 mg/mL, 30  $\mu\text{L}/\text{well}$ ) was added to each well, and further plates were allowed to incubate for 4 h at 37 °C. Subsequently, after 4 h plates were centrifuged at 2500 rpm for 5 min, the supernatant was discarded, and DMSO (100  $\mu\text{L}/\text{well}$ ) was added to solubilize the precipitated formazan. Accordingly, cell viability was measured at 540 nm using an Elisa plate reader. All experiments were repeated thrice with each drug being used in triplicates.

### Experimental Data Analysis

The parasite growth inhibition is determined by comparing the activity of control wells (normal activity) with that of treated wells (inhibited activity) via the equation.

$$\% \text{Inhibition} = \text{OD of control well} - \text{OD of treated well} * 100 / \text{OD of control well}$$

All results were represented as  $\text{IC}_{50} \pm \text{SD}$  and were calculated by linear interpolation as given below:

$$\log (\text{IC}_{50}) = \log (X1) + (50 - Y1) / (Y2 - Y1) [\log (X2) - \log (X1)]$$

where X1 = drug concentration giving % parasitic inhibition, X1 > 50%, X2 = drug concentration giving % parasitic inhibition, Y2 < 50%; Y1 and Y2 are respective cell densities (control and test).

## Results

### Photo Induced Synthesis of Silver Nanoparticles (AgNPs)

An observation about the color of the reaction mixture was made that it became darker with the increase in exposure time. There was a change in the physical appearance of the solution, which was marked by the rise in the intensity of the solution's color to deep red-brown color. There was a continuous rise in the UV-absorbance of the reaction mixture at around 415 nm, with respect to time. Also, the maxima of the peak observed for absorbance of the reaction mixture to exposed sunlight for different durations showed a blue shift. This showcases the biosynthesis of AgNPs with the passage of time. The intensity of the surface plasmon resonance (SPR) band was elevated for up to 15 min; after that, it ceased to increase. Whereas further, no change in the intensity of the SPR band was observed, indicating the termination of the synthesis process. Conclusively, 10 min was marked as the optimum time of exposure to sunlight in the photo-induced synthesis of AgNPs (Fig. 1A).

### Effect of Varying Concentrations of $\text{AgNO}_3$

The color of the reaction mixture became darker with the continuing increase in  $\text{AgNO}_3$  concentration at the fixed reaction time. Our observation showed that when  $\text{AgNO}_3$  concentration increases, the peak maxima also increase correspondingly (Fig. 1B). The spectra showed that the concentration of 3 mM showed a good SPR band, indicating the proper formation of nanoparticles.

### Effect of the Aqueous Extract (AE) Initial Dose

The findings stated that while increasing the AE dose, the sharpness and intensity of the SPR band continued to increase up to 1000  $\mu\text{l}$  and later stopped. From 200 to 1000  $\mu\text{l}$  of AE formed a shoulder peak and increased intensity towards the blue region. This signifies that the formation of nanoparticles increased with an increase in AE inoculum dose up to 1000  $\mu\text{l}$  (Fig. 1C). Thus, 1000  $\mu\text{l}$  was considered the optimum dose of the AE for nano synthesis.

### Characterization of the Green Synthesized AgNPs

#### FTIR-ATR

The combined FTIR spectra of both the AE and the AgNPs are shown in Fig. 2A. The AE shows the peaks at 2821



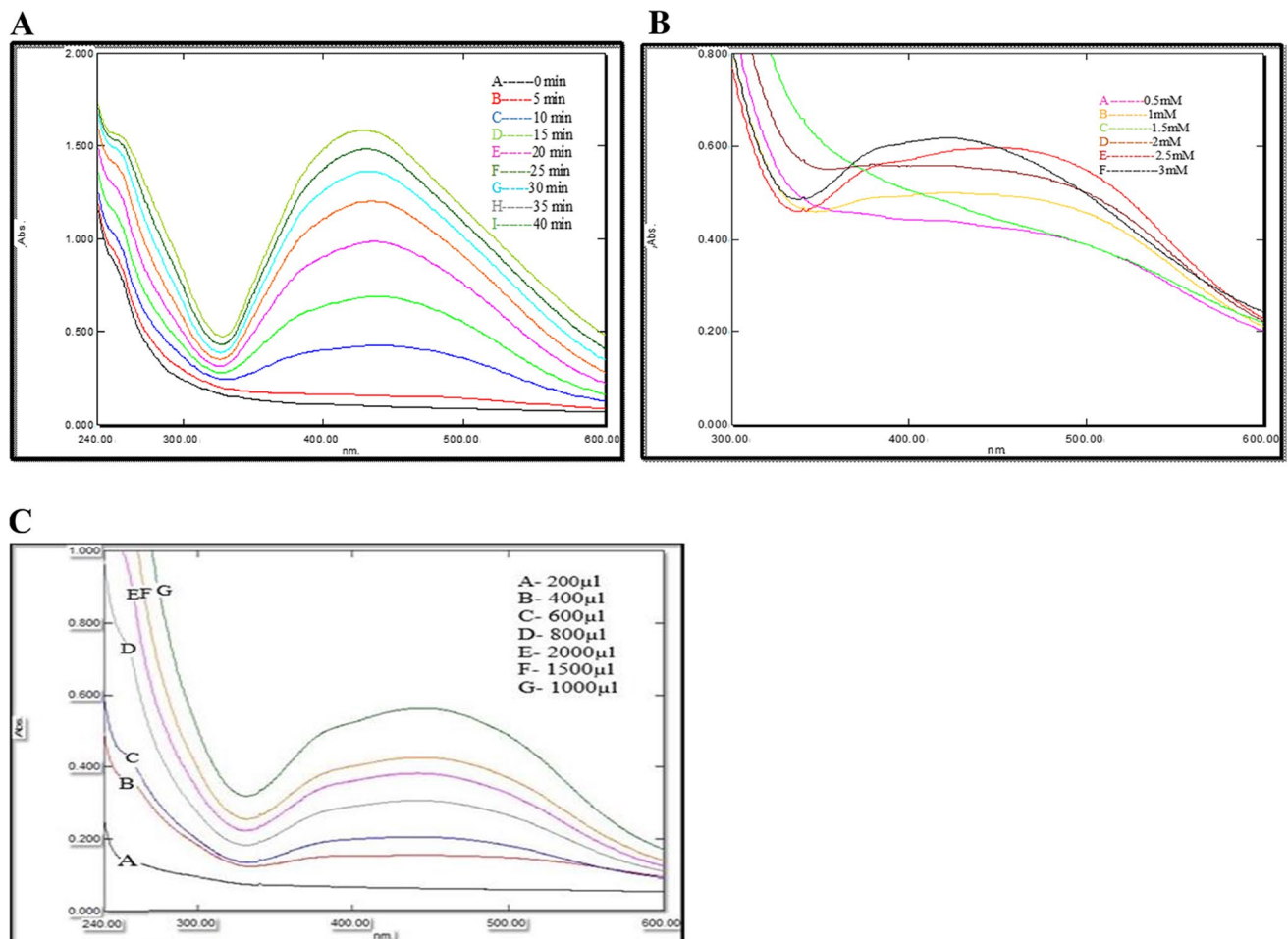


**Fig. 1** Green synthesis of silver nanoparticles (AgNPs) using *Ascophyllum nodosum* aqueous extract by the photo-induced method. **A** UV absorbance of the reaction mixture with respect to the time duration of sunlight exposure. The curve-D (15 min) showed the maxi-

um absorbance. **B** Green synthesis of AgNPs at different concentrations of AgNO<sub>3</sub>. The curve-F (3 mM) showed maximum absorbance. **C** Green synthesis of AgNPs at different inoculum dose of aqueous extract. Curve-G (1000 µl) showed the maximum absorption

$\text{cm}^{-1}$ , 2389  $\text{cm}^{-1}$ , 2371  $\text{cm}^{-1}$ , 1756  $\text{cm}^{-1}$ , 1638  $\text{cm}^{-1}$ , 1521  $\text{cm}^{-1}$ , and 1491  $\text{cm}^{-1}$ . After reduction, 7 spectral peaks of AE slightly shifted to 2876, 2375, 2334, 1739, 1634, 1537, and 1514  $\text{cm}^{-1}$  which appeared exactly at a location in AgNPs. The 2821  $\text{cm}^{-1}$  peak showed C-H stretch strong by the alkyne groups in the extract. This peak was reduced to a much lower intensity at 2876  $\text{cm}^{-1}$  of AgNPs spectra. This observation was probably due to the fact of transmission to quinonoid form from the enol form of the polyphenols present in the AE during the biosynthesis of AgNPs (Kumar et al., 2016). The IR peak at 2876  $\text{cm}^{-1}$  of the AE was due to aldehydic C-H stretching. The diminishing of this peak in the AgNPs spectra shows that the reduction of AgNO<sub>3</sub> occurred due to an aldehydic group's involvement took [16]. The strong peak at 1634, 1537, and 1514  $\text{cm}^{-1}$  was due to C=O, aromatic nitro compound stretching of a primary amide group. This characteristic peak indicates the presence of amino acids in the AE, which were used

in the stabilization of AgNPs [17]. These results indicate that the AE has constituents acting as a capping agent for the formation of AgNPs.

#### HRSEM and EDX Analysis

Spherical AgNPs were synthesized as confirmed by high resolution-scanning electron microscopy and the size ranged between 36 and 69 nm (Fig. 2 B). Some big-sized nanoparticles were seen, which could be because of the accumulation or overlapping of the particles. Synthesis of AgNPs was evidenced by the EDX spectra that were determined between 2 keV and 4 keV, which evidently displayed a strong spectral signal in the silver region at 3.5 keV (Fig. 2C). In EDX spectra, the presence of signals of carbon, oxygen, and sodium signals the presence of AE's bioactive compounds indicated. This result supports the presence of AE as a capping agent with the nanoparticles.

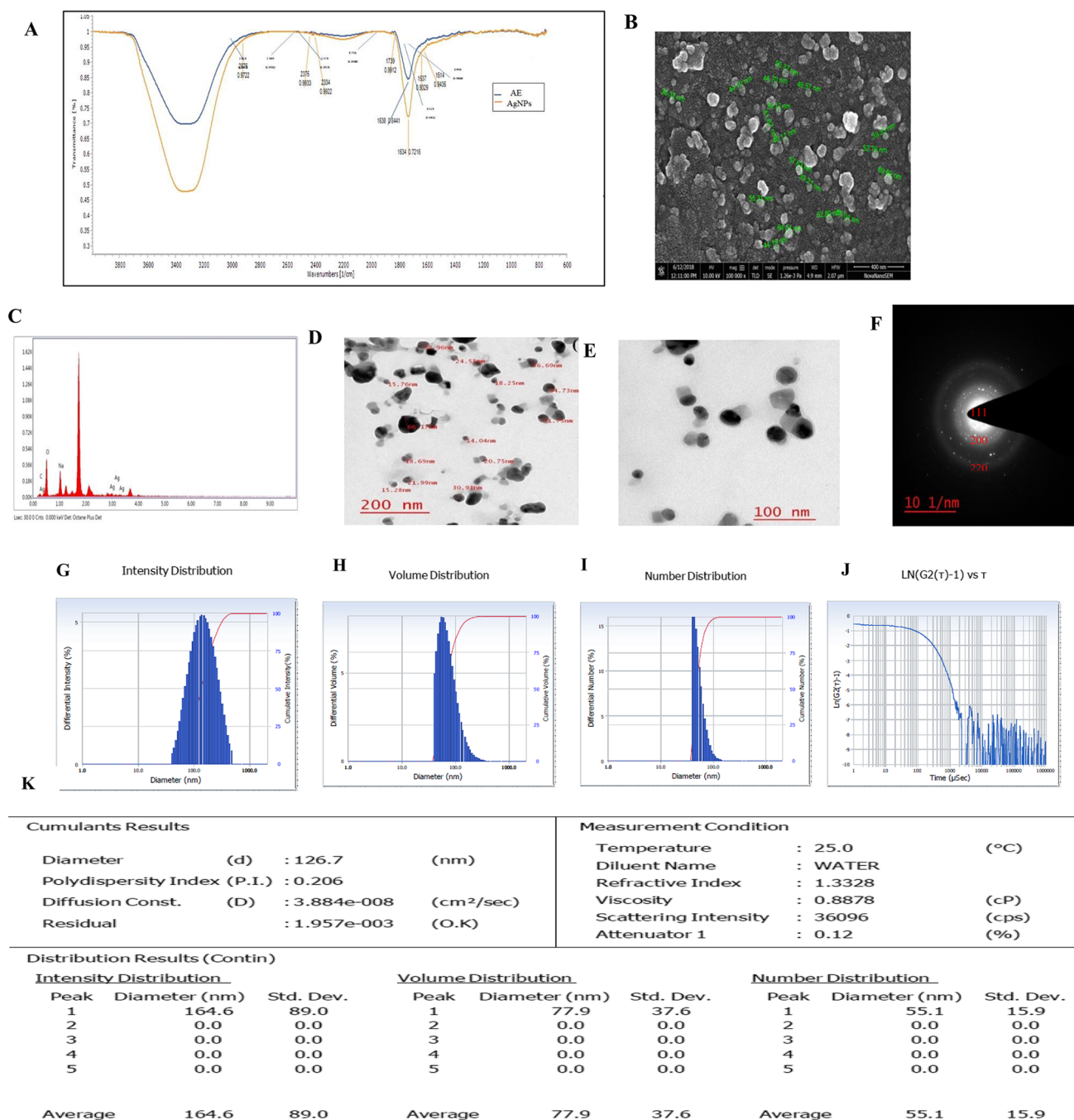


**Fig. 2** Characterization of the green synthesized silver nanoparticles (AgNPs). **A** FTIR ATR spectra of AE and AgNPs. **B** HRSEM image of silver nanoparticle with 100,000X magnification. **C** EDX analysis of silver nanoparticles. **D** HR-TEM images of AgNPs at 200 nm. **E** HR-TEM images of AgNPs at 100 nm. **F** Selected area electron diffraction (SAED) pattern of AgNPs. **G** Intensity distribution of silver nanoparticles (AgNPs) in particle size analysis. **H** Volume distribution of silver nano particle in particle size analysis. **I** Number distribution of silver nano particle in particle size analysis. **J** Light scatter of AgNPs in particle size analysis. **K** Cumulative result during particle size analysis. **L** XRD pattern of photo-synthesized AgNPs.

**M** Lateral view image of silver nanoparticle through AFM. **N** 3D view image of silver nanoparticle through AFM. **O** roughness profile in AFM. **P** XPS spectrum of the AgNPs differ from 0 to 600 eV. **Q** High-resolution XPS (HR-XPS) of binding energy (BE) of Ag 3d region of the reaction mixture is portrayed. **R** XPS spectra for the N (1s) region, also, the binding energies observed at 399.8 eV are attributed to the strong interaction between the AgNPs and the organic compounds with multiple amine groups presents in the AE. **S** XPS of the O (1s) region. **T** The C (1s) spectrum parallel to the bonds of the carbon atoms

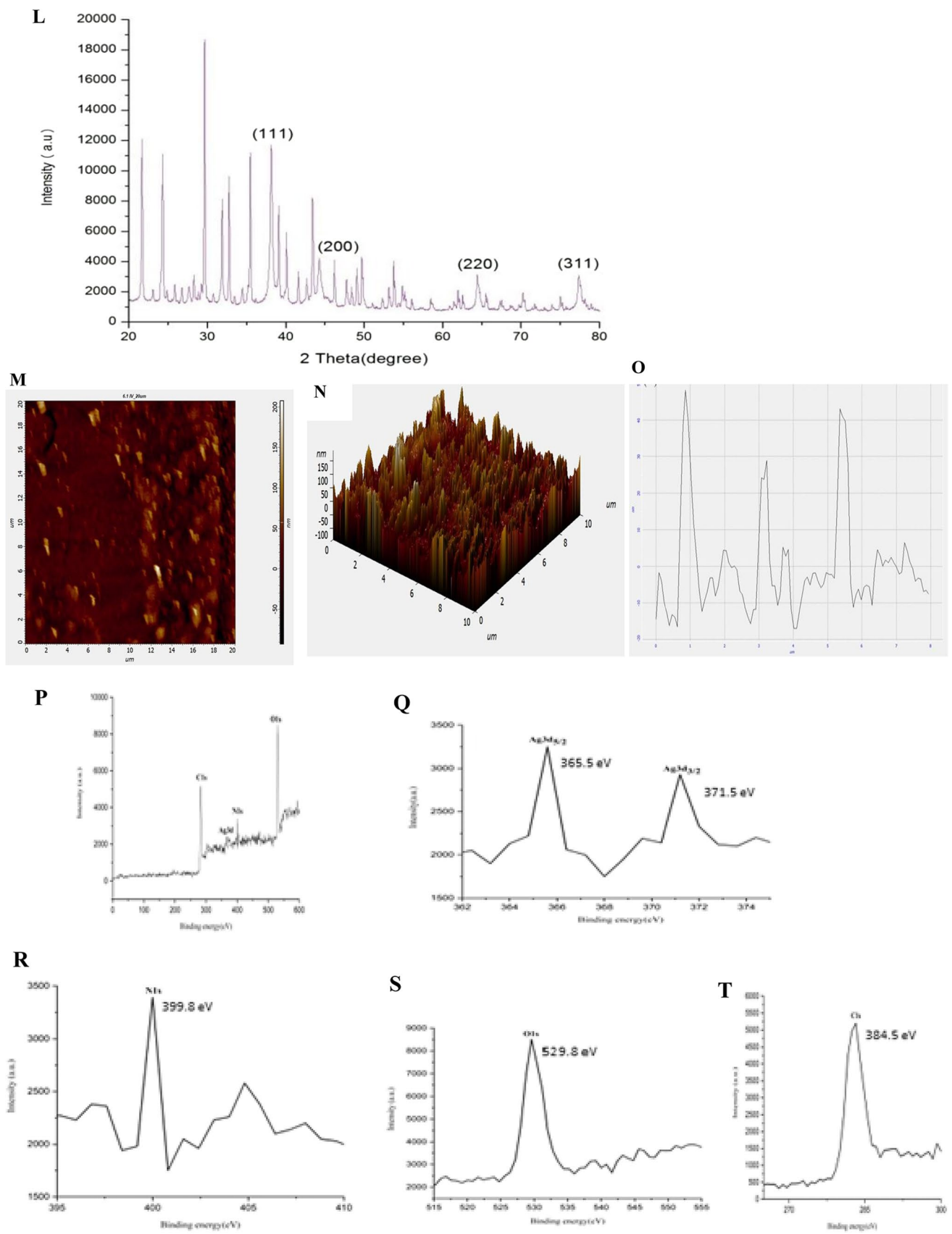


Fig. 2 (continued)



## High Resolution-Transmission Electron Microscopy (HRTEM) Analysis

HRTEM images of the AgNPs are shown in Fig. 2D and E. Nanoparticles with spherical shapes and smooth surfaces prove to be very stable. Analysis of the selected area electron diffraction (SAED) pattern as shown in Fig. 2F confirms the crystalline nature of the AgNPs. The particle size distribution of AgNPs was between 14 nm and 30 nm, with an average particle size of 27 nm.

## Particle Size Analysis

A dynamic light scattering method was adopted to analyze the particle sizes to give a picture of the particle size distribution of the synthesized AgNPs (Fig. 2G–K). Particles of various sizes ranging from 55.1 to 126.7 nm were observed. The average particle size for AgNPs was found to be 164.6 nm. The particle size analyzer showed the occurrence of AgNPs with low polydispersity index, PDI (0.206). The average particle size and PDI exhibited that the produced AgNPs are monodispersed.

## X-Ray Diffraction Analysis of AgNPs

XRD examination was done to understand the crystalline nature of dried AgNPs. The obtained XRD pattern of AgNPs was given in Fig. 2L. Formation of four distinct diffraction peaks is seen at the  $2\theta$  range of 38.17, 44.27, 64.42, and 77.47, respectively, corresponding to 111, 200, 220, and 311 the planes of face-centered cubic crystal structure of metallic silver (joint committee on powder diffraction standards-JCPDS file no.00-004-0783). *Debye-Scherrer* equation has been reported in the literature for checking the average particle size of the AgNPs,

$$D = \frac{K \lambda}{\beta \cos \theta}$$

$D$  = average crystallite domain size, perpendicular to the reflecting planes;

$K$  = Scherrer's constant (value from 0.9 to 1);

$\lambda$  = wavelength of the X-ray source (0.1541 nm) used in XRD,

$\beta$  = full width at the half maximum of the diffraction peak, and  $\theta$  is the diffraction angle. In accordance to the *Debye-Scherrer* equation, 20 nm is said to be the average particle size.

## Atomic Force Microscopy Analysis

AFM is regarded as an ideal tool for the characterization of the texture of particle surface and particle size distributions of the produced nanoparticles. Based on the AFM study, 2D (Fig. 2M) and 3D (Fig. 2N) pictures of AgNPs were recorded. Based on the analysis, the average surface roughness of AgNPs was calculated as 9.359 nm. The results depicted the maximum profile peak height and valley depth as 48.187 nm and 40.818 nm, respectively (Fig. 2O).

## XPS Analysis

X-ray photoelectron spectroscopy is carried out to assure the chemical state, and near-surface composition of the AgNPs obtained from AE. XPS spectrum of the AgNPs differs from 0 to 600 eV (Fig. 2P). Silver [Ag 3d], carbon [C (1s)], nitrogen [N (1s)], and oxygen [O (1s)] elements were identified. High-resolution XPS (HR-XPS) of binding energy (BE) of the Ag 3d region of the reaction mixture is portrayed in Fig. 2Q. Peaks placed at 365.5 eV and 371.5 eV depict Ag 3d region. Two peaks arise because of the spin-orbital splitting that corresponds to Ag 3d<sub>5/2</sub> and Ag 3d<sub>3/2</sub> core levels. Figure 2R displays the XPS spectra for the N (1s) region. Also, the binding energies observed at 399.8 eV are attributed to the strong interaction between the AgNPs and the organic compounds with multiple amine groups present in the AE. This finding aligns with FTIR results. Figure 2S illustrates the XPS of the O (1s) region. An intensity at 529.8 eV in the O (1s) region corresponds to the bond Ag—O. Strong contact between a vacancy in the *d*-orbital of Ag and organic molecules in AE leads to the formation of the bond Ag—O. Lastly, Fig. 2T demonstrates the C (1s) spectrum parallel to the bonds of the carbon atoms. According to this, an intensity of 284.5 eV can be credited to the C—O bond.

## DPPH(2,2-Diphenyl-1-Picryl-Hydrazyl-Hydrate) Radical Scavenging Assay

The percentage inhibition values for DPPH radical scavenging activity of both AE and AgNPs are shown in Table 1. The AgNPs (IC<sub>50</sub> = 103.79 µg/ml) exhibited far greater free radical scavenging ability the AE (IC<sub>50</sub> = 765.92 µg/ml).

## In Vitro Anti-Fungal Activity

The disc diffusion assay exhibited an inhibited growth of the inoculums, surrounding the samples (Fig. 3). The fungal growth was inhibited in both the species, by both AE and AgNPs, showing a clear zone of inhibition. This outlines the anti-fungal ability of both the AE and AgNPs. The values of the zone of inhibition are given in Table 2. Moreover, the AgNPs exhibited a greater fungal inhibitory effect, than the AE. Interestingly, the MIC value of

**Table 1** DPPH Radical scavenging assay of aqueous extract and silver nanoparticles

Concentration (µg/ml)	Percentage inhibition of AE (mean ± S.E)	Percentage inhibition of AgNPs (mean ± S.E)
50	10.044 ± 0.47**	2.674 ± 0.72**
100	14.032 ± 0.99**	8.024 ± 0.52**
200	25.892 ± 1.15**	6.872 ± 1.54**
400	26.770 ± 1.32**	21.193 ± 1.33**
600	64.060 ± 1.01**	30.041 ± 1.91**
800	72.990 ± 1.10**	36.213 ± 1.89**
1000	77.232 ± 1.33**	51.028 ± 1.21**
IC <sub>50</sub>	765.92µg/ml	103.73µg/ml

IC<sub>50</sub> value of ascorbic acid = 89.10

\*\* Significant at *P* value < 0.001

AgNPs was 8 times lesser than the AE in both species (*C. albicans* and *C. tropicalis*). Furthermore, the MFC values of AgNPs were also much lesser than the AE. This result shows a significant anti-fungal ability of the AgNPs, in contrast with the AE of *Ascophylum nodosum*. The values of MIC and MFC are listed in Table 2.

### Cytotoxicity Study (Splenocyte)

Plant extract with 20, 80, and 100 µg/ml concentration show 88, 47, and 42% splenocyte cell viability, respectively, following 1 h of incubation of pre-treated cells (Fig. 4A). However, NPs with 20, 40, 80, and 100 µg/ml concentration show 88, 66, 42, and 34% splenocyte cell viability, respectively, post 1 h of incubation of pre-treated cells (Fig. 4B). In comparison to plant extract, NPs shows slightly more toxicity at higher dose such as 80 µg/ml dose and above concentrations. This concludes that up to 40 µg/ml of freshly synthesized NPs are very less cytotoxic to splenocyte cells and could be considered an accepted dose for therapy.

### Anti-leishmanial Activity

#### Effects of AgNPs on the Proliferation of *L. Donovanii* Promastigotes

The proliferation of *L. donovani* promastigotes was investigated in cases of AE and AgNPs treatment and also

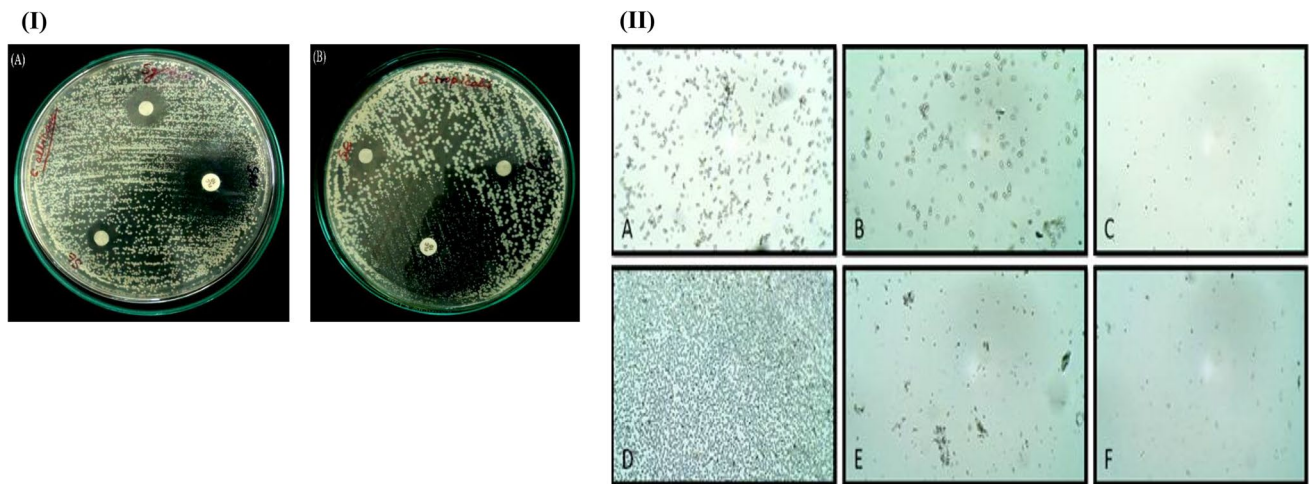


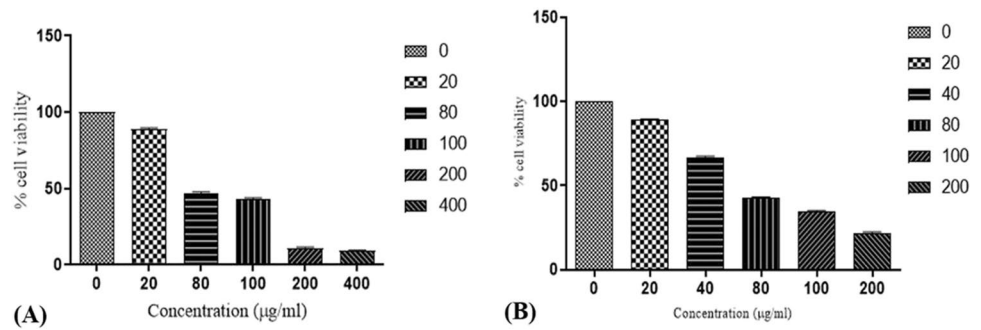
**Fig. 3** Anti-fungal activity. **(I)** Disc diffusion method to assess anti-fungal ability. Here, “Std” denotes standard, “Se” denotes aqueous extract, and “Sg” denotes silver nanoparticles. **A** Plate culture of *Candida albicans* with test samples. **B** Plate culture of *Candida tropi-*

*calis* with test samples. **(II)** **A** *Candida albicans* control. **B** Extract treated. **C** Silver nano. **D** *Candida tropicalis* control. **E** Extract treated. **F** Silver nano treated

**Table 2** S.I. of intra-macrophage amastigotes calculated by the ratio between CC<sub>50</sub> and IC<sub>50</sub> of macrophage amastigote forms

Compound	Mol. wt.	IC <sub>50</sub> (µM) on promastigote forms of <i>L. donovani</i>	IC <sub>50</sub> (µM) on <i>L. donovani</i> intra-macrophage amastigotes forms	CC <sub>50</sub> (µM) on RAW 264.7 macrophage	SI (CC <sub>50</sub> /IC <sub>50</sub> of intra-macrophage amastigotes forms)
Aqueous Extract		42.01	52.48	<200	3.67
Silver nanoparticles		5.86	5.89	<200	33.95
Miltefosine	407.568 g/mol	7.2	8.1	<100	12.34

**Fig. 4** Cytotoxicity assay (splenocyte cells). **A** Plant extract with 20, 80, and 100  $\mu\text{g/ml}$  concentration, following 1 h of incubation of pre-treated cells. **B** NPs with 20, 40, 80, and 100  $\mu\text{g/ml}$ , post 1 h of incubation of pre-treated cells



compared with the anti-leishmanial drug, Miltefosine. The promastigotes in the control group not exposed to any treatment appeared to have intact normal cell morphology along with showing active proliferation. However, cell density in cells treated with AE, AgNPs, or miltefosine significantly decreases (Fig. 5).

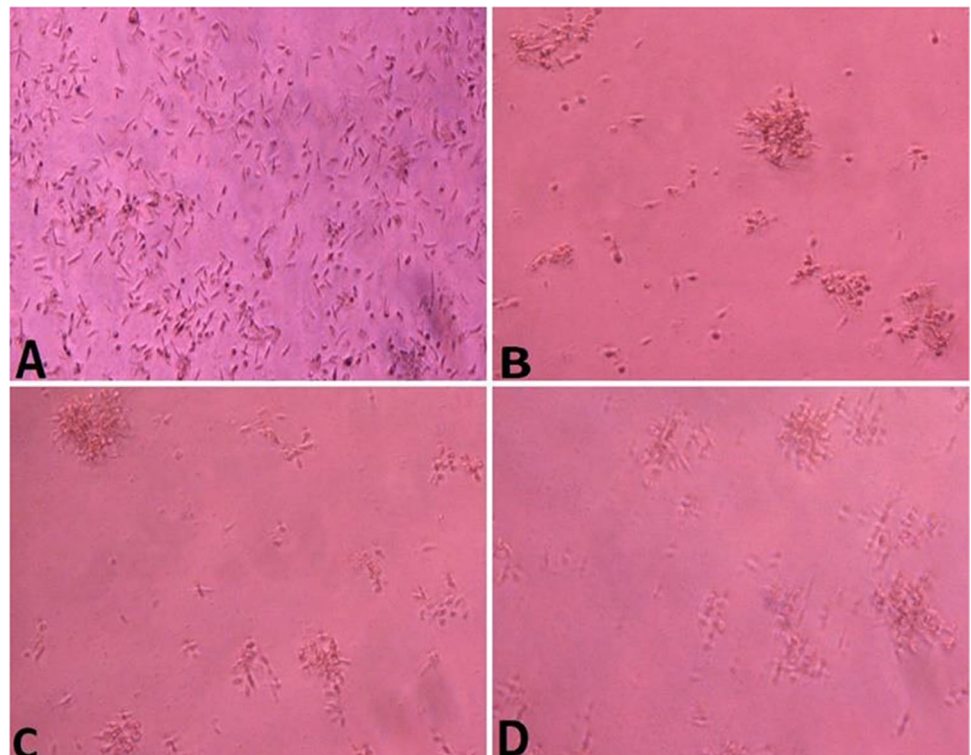
#### Percent Cell Viability on *L. Donovanii* Promastigotes

AE and AgNPs both displayed irregular cell growth, but AgNPs are perceived to be more effective. Toxicity was directly proportional to the dose as we observed more toxicity at a higher dose (200) which was not the case at a lower dose. Thus, AgNPs at lower dose show promising results in terms of being less toxic and safe (Fig. 5A and B).

#### Effect of AgNPs on Infectivity of *L. Donovanii* Amastigotes

Another biological aspect of the infectivity of *Leishmania* parasites, being the major cause of Leishmaniasis, was evaluated. Macrophages infected with *L. donovani* and the in vitro anti-amastigote activity of AgNPs and AE were analyzed. Active infection of macrophages by *L. donovani* promastigotes in control cells was seen in the promastigotes actively transformed into amastigotes. Macroscopic images of *L. donovani* promastigotes exposed to AE infected the macrophages less efficiently than they did in the control group. Further decrease in infection of promastigotes in macrophages is observed in AgNPs treated group as compared to Miltefosine-treated group (Fig. 5C and D). These results indicate that infectivity ratios of *L. donovani* amastigotes reduce

**Fig. 5** Anti-leishmanial activity of silver nanoparticles (AgNPs) on *Leishmania donovani* Promastigote in (A) control group (not exposed to silver nanoparticles [Ag-NPs] or aqueous extract [AE]) (B) AE treated group (C) AgNPs treated group and (D) Miltefosine treated group



when treated with AE, but complete inhibition of infection is observed in the AgNPs treated group Figs. 6 and 7.

### Cytotoxicity Assay (Anti-Leishmanial)

IC<sub>50</sub> values of AE and AgNPs were calculated on promastigote forms of *L. donovani* as well as *L. donovani* intra-macrophage amastigote forms. It was higher on amastigotes (52.48 μM) as compared to on promastigote forms (42.01 μM) as shown in Table 2. The IC<sub>50</sub> values for AgNPs were interestingly similar on both promastigote and amastigote forms and much comparable to the standard drug, miltefosine that we used. Furthermore, we estimated the ratio of a toxic concentration of an AE and AgNPs against its effective bioactive concentration on intra-macrophage amastigotes forms, also known as the selectivity index (SI). The window between the

cytotoxicity and anti-leishmanial activity depends on the SI value and is directly proportional to its efficacy in vivo. The SI value of the green synthesized AgNPs was maximum and almost three-fold higher than miltefosine. This proves the potent anti-leishmanial activity of our fabricated AgNPs.

### Discussion

The physical alteration confirmed the formation of AgNPs in the presence of sunlight in the color of the reaction mixture. The intensity of the colored solution increases with passing time due to the reduction of the Ag ion. The phytochemicals of AE used are responsible for the capping of the ion to prevent aggregation. This fundamental phenomenon behind the color change is SPR, which occurs due

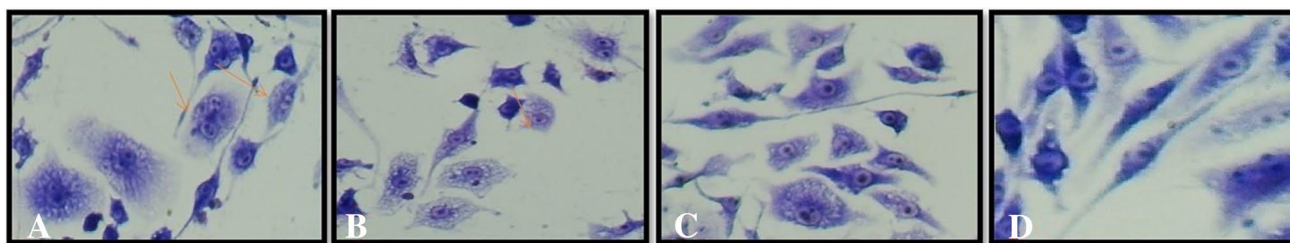
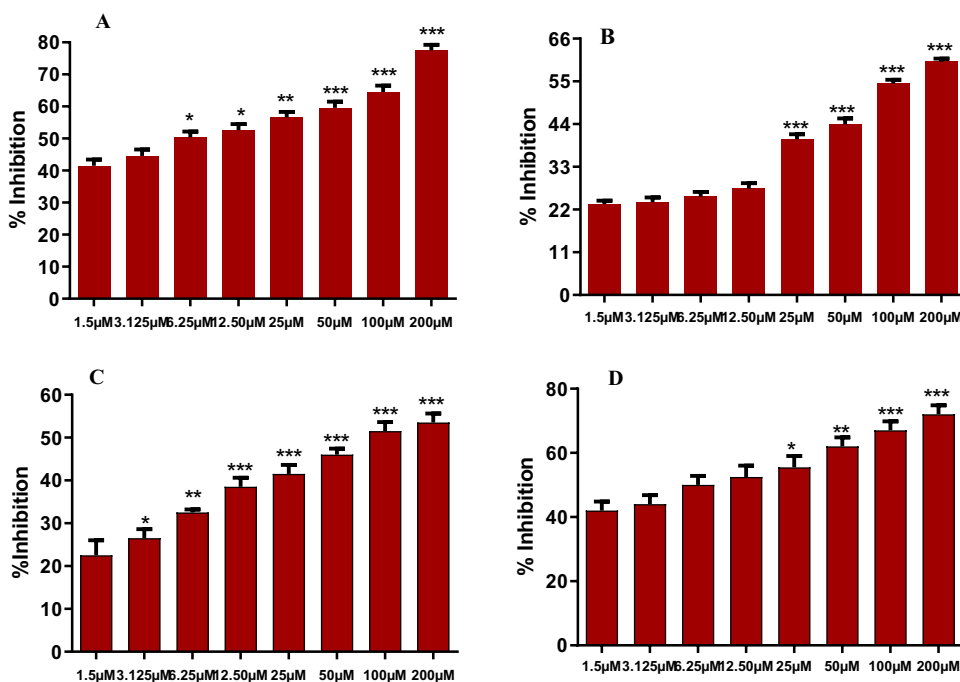


**Fig. 6** Microscopic images of macrophages infected or not infected by parasites after being stained with Giemsa. *L. donovani* promastigotes in **A** control group (not exposed to silver nanoparticles [Ag-NPs] or aqueous extract [AE]). **B** *L. donovani* promastigotes exposed to AE

treated group and **C** AgNPs treated group infected macrophages, but their infectivity was very low compared with the control group and is comparable with **D** Miltefosine treated group

**Fig. 7** Percent cell viability on *L. donovani* promastigotes exposed to **A** aqueous extract (AE) and **B** silver nanoparticles (AgNPs). Percent cell viability on *L. donovani* amastigotes exposed to **C** AE and **D** AgNPs





to the oscillations of the free electrons [18]. Additionally, the SPR effect is dependent on the nature, shape, and size of the nanoparticles. The UV-visible spectrophotometer, used for spectral characterization of the nano-sized particles, identifies the intensity of the SPR band by measuring the SPR absorbance. The AgNPs exhibited a characteristic SPR band, where the  $\lambda$  max values range from 400–500 nm [19]. We obtained the peak intensity of the SPR band at 415 nm (Fig. 1), which indicated a characteristic SPR of the AgNPs.

The characterization of AgNPs in this study also obey the Mie's theory which says that the presence of a single SPR band indicates the formation of spherical AgNPs. Observation of two or more SPR bands shows variation in the shapes of AgNPs [20]. A uniform population of spherical AgNPs as indicated by one band only was successfully synthesized. This was further supported by the HR-TEM and HR-SEM images depicting spherical and stable particles (Fig. 2B and D).

Sunlight-driven protocol of nanoparticles occurs because of the superoxide from photoirradiation which converts Ag to AgNPs. The exposure time of to sunlight to the reaction mixture for the synthesis of desirable nanoparticles also plays an avital role. It was noted that up to 15 min, the intensity of the SPR band increased, which is clear evidence of the fact that the process of formation of the particles does not go beyond a time duration of 15 min and eventually terminates. An SPR band of maximum intensity at 15 min indicated the synthesis process of AgNPs due to the reduction of  $\text{Ag}^+$  ions to  $\text{Ag}^0$ . Beyond this, the intensity saturated depicts the stopping of the synthesis process.

The two main components for the synthesis of these nano-sized particles include the  $\text{AgNO}_3$  and the AE of the plant that was used. The quality of nanoparticles synthesized depends on these two constituents' concentration. The size to a distribution ratio of the nanoparticle, referred to as the polydispersity index (PDI), is an important factor for determining the uniformity of nanoparticles. Mie's theory further stated that the chances of production of polydispersed AgNPs increase with a higher concentration of the inoculum, and even the SPR band may get split [20]. For the production of nanoparticles of fine quality, the protocol was standardized by initially optimizing the dose of inoculum. The reaction mixture with 1000  $\mu\text{l}$  of AE showed maximum absorbance. At a dose higher than 1000  $\mu\text{l}$ , the formation of a non-uniform population of particles showed a band with low intensity. In a similar manner, the concentration of  $\text{AgNO}_3$  was also optimized. An intensity maximum was obtained with a 3 mM concentration of  $\text{AgNO}_3$ . Hence, 3 mM was found to be the appropriate concentration of  $\text{AgNO}_3$  for the synthesis of AgNPs.

The particle size is analyzed by the dynamic light scattering method which depicts the particle size distribution

of the synthesized AgNPs by the AE. The range of 55.1 to 126.7 nm of the particle size distribution of AgNPs indicated the presence of various sizes of the particles. The average particle size for AgNPs was 164.6 nm, and PDI showed that the produced AgNPs were monodispersed.

Vijay kumar et al. hypothesized the mechanism behind the synthesis of nanoparticles under sunlight [21]. The photon energy from the sun is absorbed by the polyphenolic-rich AE and gets excited to a higher state by substituting its O-H groups with  $\text{Ag}^+$  ions. The monovalent cation  $\text{Ag}^+$  ions get reduced to leading to its nucleation in the formation of nanoclusters. The stability of the AgNPs is achieved due to the polyphenolic protein in the AE that acts as a capping agent [22]. This capping activity of the AE was verified by spectral signal at 3.5 keV in obtained EDX spectra (Fig. 2C) of AgNPs that showed the presence of elements of the AE, along with the AgNPs. With this, a successful method of preparation of stable AgNPs using *A.nodosum* as a capping agent is reported. Thus, the AE-coated AgNPs are advantageous compared to those prepared by other physical and chemical methods as it is shown to produce stable and spherical nanoparticles in an eco-friendly way, eliminating toxic chemicals.

The natural antioxidants have prophylactic and therapeutic effects for combating many diseases like cancer, cardiovascular disease, and age-related diseases [22]. DPPH assay is an ideal and easy method for the evaluation of antioxidant ability. This method is commonly used to evaluate the radical scavenging ability in vegetables, brans, linoleic acids, and herbs [23]. An antioxidant reduces or in other terms, scavenges the DPPH free radical. The AgNPs synthesized exhibited satisfactory free radical scavenging ability, showing better efficacy than the AE. The  $\text{IC}_{50}$  value of the AgNPs was somewhat nearer to the standard value which adds to its antioxidant potential. Various other methods can be adopted further prove its properties like superoxide radical scavenging, lipid peroxidation activity, and reducing power ability with subsequent in vivo studies.

There are several factors involved in showing the reduced microbial, fungal, and leishmanial activity by in vitro method. Previously in numerous reports, it is mentioned the capping/coating of the formulation by size reduction method in silver/metal nanoformulation has shown a more inhibitory effect, cost-effectiveness, and safer [24]. In wound dressing, Ag NPs are being used increasingly, as catheters and various household products due to their antimicrobial activity. There are several fields where AgNPs are used as antimicrobial agents extremely in textile, medicine, water disinfection, and food packaging. The antimicrobial characteristics of inorganic NPs add more potency to this important aspect than organic compounds, which are relatively toxic to biological systems [25]. The potent anti-leishmanial activity was witnessed in both AE and AgNPs. The dose-dependent



activity was found in promastigote as well as amastigote.  $IC_{50}$  in both AE and AgNPs was 42.01 and 5.86 respectively and were found effective in promastigote as compared to the standard (7.2). A similar trend of 52.48, 5.89, and 8.1 was observed in amastigote for AE, AgNPs, and standard respectively.

In conclusion, plant extract-mediated synthesis of nanoparticles has filled the void of the need for a safer method for our ecosystem. The medical field researchers find the utmost potential in these nanoparticles being utilized for drug delivery and other healthcare products. Besides this, for good implications and properties study, specific characterization techniques should be used. More importantly, environmental issues should be taken into account before using these materials for any applications, especially in the case of heavy metals, which are prone to environmental hazards and can also affect the living as well. In this study, AE of *A. nodosum* served as a capping and stabilizing agent for photo-induced synthesis of AgNPs of 30–60 nm in size. The microstructural analysis revealed the crystalline nature of the particles. The synthesized AgNPs showed remarkable DPPH radical scavenging ability owing to their antioxidant properties. The anti-leishmanial activity was exceptionally viable in both AE and AgNPs. A low dose of AE and AgNPs is considered safe for use. These findings all together support the tendency of *Ascophyllum nodosum* to efficiently synthesize AgNPs which could be utilized for its anti-leishmanial properties.

**Acknowledgements** We are very much thankful to scientists from Canada for sharing the processed sample of *Ascophyllum nodosum*. We are also thankful to the staff of the Central Instrument Facility, Indian Institute of Technology, BHU, and Department of Botany, Banaras Hindu University Varanasi.

**Author Contributions** Conceptualization and methodology: Sunil Kumar Mishra, Kavindra Nath Tiwari, Rakesh Singh, Sri Krishna, and Alok Tripathi; experimentation, data curation, investigation: Saket Sinha, Amit Kumar Singh, Pradeep Kumar, Rajan Singh, Arvind Kumar, Brijesh Singh Chauhan; writing—original draft, review, and editing: Prabhat Upadhyay and Diya Kalra; manuscript checking: SKM and KNT. All authors have read and agreed to the published version of the manuscript.

## Declarations

**Ethics Approval and Consent to Participate** The authors carried out no animal or human studies for this article.

**Conflict of Interest** The authors declare no competing interests.

## References

- Moradi F, Sedaghat S, Moradi O, Arab SS. Review on green nanobiosynthesis of silver nanoparticles and their biological activities: with an emphasis on medicinal plants. *Inorg Nano-Metal Chem.* 2020;51:133–42.
- Xu L, Wang YY, Huang J, Chen CY, Wang ZX, Xie H. Silver nanoparticles: synthesis, medical applications and biosafety. *Theranostics.* 2020;10(20):8996–9031.
- Singh J, Dutta T, Kim KH, Rawat M, Samddar P, Kumar P. Green synthesis of metals and their oxide nanoparticles: applications for environmental remediation. *J Nanobiotechnology.* 2018;16(1):84.
- Lotfollahzadeh R, Yari M, Sedaghat S, Delbari AS. Biosynthesis and characterization of silver nanoparticles for the removal of amoxicillin from aqueous solutions using *Oenothera biennis* water extract. *J Nanostructure Chem.* 2021;11:693–706.
- Upadhyay P, Mishra SK, Purohit S, Dubey GP, Singh Chauhan B, Srikrishna S. Antioxidant, antimicrobial and cytotoxic potential of silver nanoparticles synthesized using flavonoid rich alcoholic leaves extract of *Reinwardtia indica*. *Drug Chem Toxicol.* 2018;42(1):65–75.
- Pereira L, Morrison L, Shukla PS, Critchley AT. A concise review of the brown macroalga *Ascophyllum nodosum* (Linnaeus) Le Jolis. *J Appl Phycol.* 2020;32(6):3561–84.
- Liu X, Luo G, Wang L, Yuan W. Optimization of antioxidant extraction from edible brown algae *Ascophyllum nodosum* using response surface methodology. *Food Bioprod Process.* 2019;114:205–15.
- Dell'Anno M, Sotira S, Rebucci R, Reggi S, Castiglioni B, Rossi L. In vitro evaluation of antimicrobial and antioxidant activities of algal extracts. *Ital J Anim Sci.* 2020;19:103–13.
- Chauhan BS, Kumar R, Kumar P, Kumar P, Sinha S, Mishra SK, et al. Neuroprotective potential of flavonoid rich *Ascophyllum nodosum* (FRAN) fraction from the brown seaweed on an A $\beta$ 42 induced Alzheimer's model of *Drosophila*. *Phytomedicine.* 2022;95:153872.
- Ertani A, Francioso O, Tinti A, Schiavon M, Pizzeghello D, Nardi S. Evaluation of seaweed extracts from *Laminaria* and *Ascophyllum nodosum* spp. as biostimulants in *Zea mays* L. using a combination of chemical, biochemical and morphological approaches. *Front Plant Sci.* 2018;9:428.
- Rawat V, Sharma A, Bhatt VP, Pratap Singh R, Maurya IK. Sunlight mediated green synthesis of silver nanoparticles using *Polygonatum graminifolium* leaf extract and their antibacterial activity. *Mater Today Proc.* 2019:911–6.
- Mm K, Mm H, Fatema N. Determination of MIC and MBC of selected azithromycin capsule commercially available in Bangladesh. *ORION Med J.* 2009;32:619–20.
- Hudzicki J. Kirby-Bauer disk diffusion susceptibility test protocol. *Am Soc Microbiol.* 2009;15:55–63.
- Mathabe MC, Hussein AA, Nikolova RV, Basson AE, Meyer JJM, Lall N. Antibacterial activities and cytotoxicity of terpenoids isolated from *Spirostachys africana*. *J Ethnopharmacol.* 2008;116:194–7.
- Hastey CJ, Dale SE, Nary J, Citron D, Law JH, Roe-Carpenter DE, et al. Comparison of *Clostridium difficile* minimum inhibitory concentrations obtained using agar dilution vs broth microdilution methods. *Anaerobe.* 2017;44:73–7.
- Irvani S, Korbekandi H, Mirmohammadi SV, Zolfaghari B. Synthesis of silver nanoparticles: chemical, physical and biological methods. *Res Pharm Sci.* 2014;9:385–406.
- Ahmed S, Ahmad M, Swami BL, Ikram S. A review on plants extract mediated synthesis of silver nanoparticles for antimicrobial applications: a green expertise. *J Adv Res.* 2016;7:17–28.
- Jain PK, Huang X, El-Sayed IH, El-Sayed MA. Review of some interesting surface plasmon resonance-enhanced properties of noble metal nanoparticles and their applications to biosystems. *Plasmonics.* 2007;2:107–18.
- Sastry M, Mayya KS, Bandyopadhyay K. pH Dependent changes in the optical properties of carboxylic acid derivatized silver colloidal particles. *Colloids Surf A: Physicochem Eng.* 1997;127:221–8.

20. Mie G. Contributions to the optics of turbid media, particularly of colloidal metal solutions. *Ann Phys.* 1976;25:377–445.
21. Kumar V, Bano D, Mohan S, Singh DK, Hasan SH. Sunlight-induced green synthesis of silver nanoparticles using aqueous leaf extract of *Polyalthia longifolia* and its antioxidant activity. *Mater Lett.* 2016;181:371–7.
22. Liu Z, Ren Z, Zhang J, Chuang CC, Kandaswamy E, Zhou T, et al. Role of ROS and nutritional antioxidants in human diseases. *Front Physiol.* 2018.;477.
23. Cheng Z, Moore J, Yu L. High-throughput relative DPPH radical scavenging capacity assay. *J Agric Food Chem.* 2006;54:7429–36.
24. Jain AS, Pawar PS, Sarkar A, Junnuthula V, Dyawanapelly S. Bionanofactories for Green Synthesis of Silver Nanoparticles: Toward Antimicrobial Applications. *Int J Mol Sci*; 2021. 22.
25. Khan II, Saeed K, Khan II. Nanoparticles: Properties, applications and toxicities. *Arab J Chem.* 2017;12:908–31.

**Publisher's Note** Springer Nature remains neutral with regard to jurisdictional claims in published maps and institutional affiliations.

Springer Nature or its licensor (e.g. a society or other partner) holds exclusive rights to this article under a publishing agreement with the author(s) or other rightsholder(s); author self-archiving of the accepted manuscript version of this article is solely governed by the terms of such publishing agreement and applicable law.